# New insight into subcritical rupture of SiC-based filaments at intermediate temperatures (400–900 °C) under air

Stephane Mazerat, Rene Pailler

Version of Record: https://www.sciencedirect.com/science/article/pii/S0955221921006014
Manuscript_d808ee3efd08f25955a477f14dead430

# New insight into subcritical rupture of SiC-based filaments at intermediate temperatures (400-900 °C) under air

S. Mazerat, R. Pailler*

Univ. Bordeaux, CNRS, CEA, SAFRAN CERAMICS, LCTS, UMR 5801, F-33600 Pessac, France

* Corresponding author. E-mail address: s.mazerat.lcts@gmail.com

## Abstract

The delayed failure of SiC fibrous reinforcement has continuously been investigated to warrant the long term performances of Ceramic Matrix Composite (CMC). Chiefly assessed on multifilament tow samples to alleviate some handling difficulties, subcritical crack growth (SCG) parameters are however ruled by structural artifacts which hinder the identification of intrinsic filament behavior. In this paper, we propose to estimate the true filament parameters for 5 fiber types from bundle behavior using a recently communicated Monte Carlo algorithm integrating flaw and stress distributions through a deterministic fracture mechanics law under Paris' formulation. So computed tow lifetime are broadly dispersed, encompassing raw data, and show a structure-dependent scale effect, revealed by $n_{filament} > n_{tow}$ where $n$ is the stress exponent. The relationship between SCG coefficient and chemical composition of the substrate is discussed and highlights the major effect of doping elements (Ti or Zr), oxygen or hydrogen content.

## Keywords

SiC fiber . Static fatigue . Bundle lifetime . Filament lifetime . Scale effect . Delayed failure distribution

**Graphical abstract**

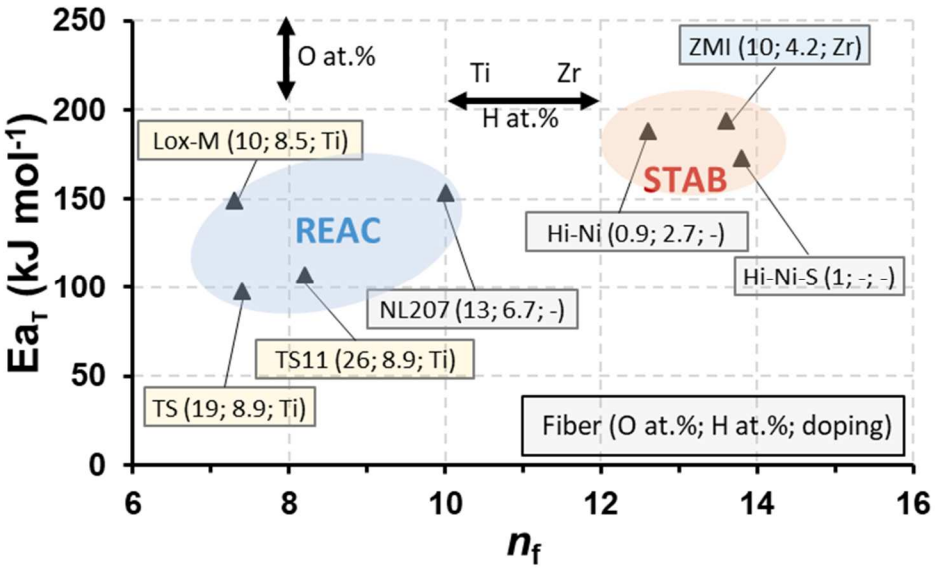


Slow crack growth parameters for SiC-based filaments. $\tau$ is the lifetime, $\sigma_{app}$ the stress, $n_f$ the stress exponent and $Ea_\tau$ the apparent activation energy describing the Arrhenius evolution of the environment constant $A$ with temperature.

# Abbreviations

This article describes mechanical and static fatigue behavior of filaments and tows with similar equations. Therefore, subscripted suffixes "*f*" or "*t*" were added to the symbols in the manuscript, to refer respectively to filament or tow. An absence of suffix indicates a generic behavior, used for both scales.

| | |
|---|---|
| $S$ | sample section, $S_t$ for tow and $S_f$ for fiber |
| $N_t$ | total number of filaments in a tow |
| $N_0$ | number of effectively loaded filament in a tow |
| $\gamma$ | fraction of unloaded bundle section |
| $w$ | force applied to the sample ($w_f$ or $w_t$) |
| $\delta_F$ | over or under-load (force) applied to a filament; $\delta_F$ can be converted to over or under-stress admitting homogeneous fiber section ($S_f$) |
| $\varsigma$ | standard deviation of $\delta_F$ applied to the $N_0$ filaments of a tow |
| $\sigma_{app}$ | stress applied to the sample ($\sigma_{app.f}$ or $\sigma_{app.t}$) |
| $\sigma_r$ | tensile strength ($\sigma_{r.f}$ or $\sigma_{r.t}$) |
| $\alpha_t$ | critical fraction of broken fibers leading to tow ruin under static fatigue test at a constant force |
| $\tau$ | time to failure under static fatigue conditions ($\tau_f$ or $\tau_t$) |
| $n$ | stress exponent ($n_f$ or $n_t$) |
| $A_1$ | environmental parameter for static fatigue ($A_{1.f}$ or $A_{1.t}$) |
| $m_\tau$ | Weibull modulus describing the distribution of delayed failures ($m_{\tau f}$ or $m_{\tau t}$). |

# 1. Introduction

Advanced ceramics are candidate materials for many applications requesting thermostructural properties. One of their limitation lies in the delayed failure they display, under the combined influence of subcritical stress and hostile (oxidizing) environment. This phenomenon has overwhelmingly been studied, since M. Grenet evidenced it in 1899 on glasses [1]. It is explained by the chemical attack of strained bonds at inherent surface flaw tips, causing cracks to slowly grow (slow crack growth, SCG) until one of them had reached the stress-dependent critical size and dramatically propagated through the material [2-13]. Ceramic Matrix Composite (CMC), such as $SiC_m/SiC_f$, suffer from the same delayed failure mechanism at intermediate (400-1000 °C range) or high temperatures (>1000 °C). Because the ultimate failure of CMC is dictated by the reinforcement [14], sensitivity of various SiC fibers to slow crack growth in oxidative environment became a key to predict and tune the composite durability. Model for this prediction is derived from the Paris-Erdogan (power) law as follows:

$$\tau = A\sigma_{app}^{-n} \quad (1)$$

where, $\tau$ is the lifetime, $\sigma_{app}$ the stress, $A$ and $n$ the SCG coefficients, respectively the environmental constant and the stress exponent. This latter, also named stress susceptibility factor, is a key parameter for the engineering of composite parts targeting long term application. On SiC-based tows, exponents ranging for 5 to 10 were reported [15-17], standing below the classical values assessed for classical oxide [18] or covalent non oxide [19-21] ceramics. These coefficients are however pertinent to the tow scale only, as revealed on Hi-Nicalon fiber type: single filaments $n_f$ = 12.6 [22], multifilament tows $n_t$ = 8.4 [15], minicomposite $n_{minic}$ = 5.4 [23] and composite $n_{comp}$ = 2 [24]. As a consequence, the intrinsic filament behavior, usefull for fundamental understanding on how the chemical composition or the microstructure can impact $n$ [25], can not be deduced from convenient tow testing. In a

recent communication, the discrepancy between $n_t$ and $n_f$ was shown to originate from combining variabilities on filament strength and stress [26]. The latter is explained by delayed strain activation of fibers due to their slack (lack of parallelism) [27]. Stochastic modelling strategies are here relevant to consider the combined effects of uncertainties as follows: first, to each bundle was ascribed a random structure, and to each filament a stress and a strength; second, the lifetime for all individual filaments was calculated and used to define the virtual tow lifetime.

This work propose to extend this methodology to other fiber types in order to estimate filament parameters from bundle behavior. Tow testing rehabilitation is obviously sought. The relationship between these parameters and substrate composition or microstructure are finally discussed, with the underlying objective to identify key factors and approximate the SCG parameters for any SiC-based fiber. Outlooks may also include virtual CMC performance assessment as proposed by [28], SiC fiber development or bundle static fatigue interpretation (not restricted to SiC). This paper is hence an attempt to consolidate the present situation on this specific topic for the wealth of experimental data analysis and subsequent CMC performance simulation.

# 2 Material and method

## 2.1 Material

Three generations of SiC-based fibers are commercially available, synthesized by the conversion of polycarbosilane (Nippon Carbon Co. Ltd. under the trade name Nicalon®), or derivate containing a small amount of organometallic (UBE Industries Ltd. named Tyranno®). The first-generation fibers are melt spun then oxygen cured and pyrolyzed at 1200-1300 °C. They are composed of a silicon oxycarbide phase (SiCO) embedding SiC grains in nanometer

range and free aromatic carbon as basic structural units [29]. Second generation fibers are however electron beam cured, hence oxygen free, and contain excess of carbon inhibiting SiC grain growth, also in nanometer range. Near stoichiometric third-generation fibers are synthesized by further heat treating (about 1800 °C) first or second-generation fibers. Constituted of coarser SiC grains (>50 nm), these fibers display good stability at high temperature [30].

In this study, 6 first-generation fibers are reported: Nicalon® NL101, NL207, Tyranno® Grade S, referred as TS, Tyranno® Lox-M, Tyranno® ZMI and Tyranno® AM. In addition, were also characterized two different batches of TS with 8.5 or 11 µm mean diameter (respectively 1600 and 800 fiber per tow). Hi-Nicalon, referred to as Hi-Ni, belongs to the second-generation whereas Hi-Nicalon Type S, called Hi-Ni-S, is a third generation SiC-based fiber completing the study. On these latter types, mechanical properties were assessed on the bathes used by W. Gauthier et. al [15] and A. Laforet [23] works. Hence a total of 9 SiC-based fiber tows are reported in this study. The microstructure and elemental composition of fibers were extracted from G. Puyoo work [31] (Table 1) compiling XRD electron microprobe and SIMS experiments. The oxygen, carbon free and hydrogen contents cover a broad range of values (respectively 0-25, 3-27 and 0-9 at.%), usefull for trend identification. It can be noticed that the amount of carbon free is not necessarly linked to the oxygen or the hydrogen contents.

| Fiber | Diameter (µm) | Number of fiber per tow | Composition (at.%) | | | | | $C_{free}$ (at.%) | Grain size (nm) | Density (g cm$^{-3}$) |
|---|---|---|---|---|---|---|---|---|---|---|
| | | | Si | C | O | Hetero-element | H | | | |
| NL207 | 14 | 500 | 36.1 | 45.3 | 11.9 | - | 6.7 | 16.4 | 1.9 | 2.58 |
| TS | 8.5 | 1600 | 29.0 | 43.8 | 17.7 | (Ti) 0.6 | 8.9 | 26.0 | 1.2 | 2.35 |
| TS11 | 11 | 800 | 28.8 | 38.0 | 23.7 | (Ti) 0.6 | 8.9 | 23.0 | 1.2 | 2.35 |
| Lox-M | 11 | 800 | 32.4 | 48.8 | 9.5 | (Ti) 0.8 | 8.5 | 23.1 | 1.9 | 2.37 |

| | | | | | | | | | | |
|---|---|---|---|---|---|---|---|---|---|---|
| ZMI | 11 | 800 | 34.0 | 52.0 | 9.6 | (Zr) 0.2 | 4.2 | 23.9 | 2.2 | 2.48 |
| Hi-Ni | 14 | 500 | 40.8 | 55.7 | 0.9 | - | 2.7 | 15.8 | 5.0 | 2.74 |
| Hi-Ni-S | 12 | 500 | 48.2 | 50.8 | 1.0 | - | 0 | 3.1 | 50 | 3.05 |
| NL101 | 15 | 500 | 34.1 | 43.9 | 15.7 | - | 6.3 | 18.8 | 1.2 | 2.57 |
| AM | 11 | 800 | 32.0 | 51.1 | 13.8 | (Al) 0.4 | 2.7 | 26.7 | 2.2 | 2.42 |

**Table 1**: Composition and physical properties of SiC-based fiber.

### 2.2 Tensile tests on monofilaments

Mechanical properties of filaments were measured at room temperature in ambient atmosphere on a dedicated tensile machine. Single fibers were randomly selected in a tow, mounted, aligned and glued on a paper holder with a 25 mm gauge window [32,33]. The diameter of each test specimen was measured by laser diffraction method. Once gripped on the testing machine, the paper holder was cut on both sides. Tensile tests were carried out under quasi-static condition, at 0.5 % $min^{-1}$. More than 40 tests were conducted on each fiber type. In addition, ten extra tests with 10 mm and 40 mm gauge lengths were carried out for machine compliance evaluation and correction of measured elongations (Table 2) [33].

### 2.3 Tensile tests on bundles

Bundle specimen preparation, described elsewhere [34], was identical for both tensile and static fatigue tests for obvious representativeness reasons. Sized bundles of 300 mm length were weighted for determination of average cross sectional area (Eq. (3)) and positioned in alumina tube grips. To ensure probe alignment, a pre-load was applied and maintained by fugitive Loctite® glue. A solution of dissolved PMMA was applied on the 25 mm gauge length separating grips to avoid capillarity cement transportation during curing. Tubes were finally filled with alumina based thermostructural cement (Ceramabond 503, Polytec PI) and cured at 370 °C for 2 hours.

Tensile tests were carried out on non-lubricated yarns at a constant displacement rate of 50 µm $min^{-1}$ (strain rate of 0.2 % $min^{-1}$) measured by two LVDT extensometers mounted on the grips. A loading-unloading cycle was applied at low load (0-30 N, in the elastic domain) in order to align the fibers and properly estimate their parallelism and the effective tow section ($\gamma$, Eq. (4)) [35]. Between 25 and 100 tests were performed on each fiber type. Three (3) more tests at 60 mm and 100 mm gauge lengths were carried out to remove the system compliance from strain and Young modulus calculation as described by ASTM 1557-03. The stress on tow inferred from Eq. (2) [36]:

$$\sigma_{app(\gamma)} = \frac{w_t}{S_t(1-\gamma)} \tag{2}$$

with $$S_t = \frac{m_0}{L_0 \rho} \tag{3}$$

and $$\gamma = 1 - \frac{N_0}{N_t} = 1 - \frac{E_t}{E_f} \tag{4}$$

where $m_0$ is the mass of a $L_0$ length tow (300 mm) with $S_t$ its section and $\rho$ the fibers density (Table 1). $w_t$ is the applied force, $\gamma$ the unloaded section fraction, $N_0$ the initial number of continuous filaments and $N_t$ is the total number of manufactured filaments in the tow (including the broken ones). Finally, $E_t$ and $E_f$ are respectively tow and monofilament Young moduli.

### 2.4 Static fatigue tests

Static fatigue tests were carried out on fiber bundles over the 400-900 °C range under ambient air in a resistive vertical furnace described in [15,34,37]. Of note, the present work focuses on sub-healing condition (temperature ≤ 900 °C), where the reinforcement behavior is expected to be more representative to predict the composite part performances. The hot grip technique was used to ensure a uniform temperature along the entire specimen gauge length. Force was applied through a dead weight suspended to inferior grip (applying a force $w_t$) turning a timer

on. Heating-up (20 °C $min^{-1}$) was then initiated and its duration subtracted from lifetime when relevant. The automatic stop of timer when specimen failed defined the tow lifetime. Were deemed as valid only those tests that run without breakage during the initial loading or heating steps (in firsts 100 seconds). Due to practical difficulties on static fatigue testing setup, force and strain could not be recorded. As a consequence, the $\gamma$ value, pertinent to the probe, could not be calculated. Its average value, assessed on the same probes by tensile test, was instead used to estimate the applied stress. This source of uncertainty was explored in a previous communication [34] and found to represent a non-negligible source of dispersion.

Studies have shown a minimum of 75 tests are needed to reliably define the median lifetime in one given condition (stress-temperature), and over 100 to estimate properly their distribution [38]. Cost and time constraints preclude that possibility. Lifetime prediction parameters ($A$ and $n$), were reasonably estimated (error <10% on $n$) considering the following method: 11 tests performed for each couple stress-temperature. To characterize the lifetime dispersion, some conditions were more extensively tested (≥30). This obviously applies for affordable conditions, leading to comfortable lifetime lying between 1 hour and 3 months.

# 3 Theory

### 3.1 Fiber bundle theory

Here, we name bundle an assembly of hundreds of fine, parallel and long fibers. Taken individually, they exhibit a brittle fracture behavior and their strength can be described by the two-parameter Weibull distribution as:

$$\sigma_{r.f} = \sigma_{1.f} \ln\left(\frac{1}{1-P_i}\right)^{\frac{1}{m_f}} \quad (5)$$

where $P_i$ is the probability that a fiber (of rank $i$) will sustain an applied stress $\sigma_r$ without breaking ($P_i = (i - 0.5) / B$) [39-41]. $m_f$ and $\sigma_{1.f}$ are respectively the Weibull modulus and the characteristic strength. $B$ is the data set size.

While tensile testing a bundle, the stress-strain curve is characterized by three phases: the loading with upward curvature indicative of progressive fiber alignment and loading however seldom exploited [27]; the linear elastic phase where $N_0$ filaments are loaded preceding the first break events [42,43]. This latter depends on loading mode: (i). when force piloted the load is redistributed (globally or locally) to surviving elements whereas (ii). when strain piloted there is no load sharing phenomenon. As a consequence, in the latter scenario all fibers will progressively and individually fail [44]. In the former testing mode however, the ultimate failure occurs when surviving fibers can not whistand the force increment, in other words when a critical number of fibers have failed. The ratio α of broken fibers to its initial number $N_0$ can be identified as the failure probability.

The loading and linear elastic domains of strain piloted tensile tests were used to define the bundle structure. The well known bundle model [45-47] was hence modified to account for fiber slack and subsequent fiber load distribution which can be expressed as follows:

$$w_{fj} = \overline{w}_f + \delta_{Fj} \quad (6)$$

where $w_{fj}$ is the load applied to the $j^{th}$ filament, $\overline{w}_f$ the mean value corresponding to the tow one ($\overline{w}_f = w_t / N_0$) and $\delta_{Fj}$ the load distribution (over or underload on $j^{th}$ filament, centered to 0 N). $\delta_{Fj}$ infers from the initial interval to linearity, assuming homogeneous elastic modulus, as:

$$\psi_{(t)} = 1 - \frac{\Delta w_{(t)}}{w_{(t)} + \Delta w_{(t)}} \quad (7)$$

where $\psi_{(t)}$ is the section fraction carrying the force, $\Delta w_{(t)}$ the difference between the applied force and the projection of the linear elastic domain described in [48]. $\psi_{(t)}$ progressively increases until 100%, when the $N_0$ fibers are loaded and the linear domain reached. This was experimentally evidenced below 30 N. The force for each strain increment, applied to the full sample, is supported by $N_t \times (1 - \gamma) \times \psi_{(t)}$ fibers. The force distribution was finally interpreted with a normal distribution as follows:

$$f(\delta_F) = \frac{1}{\varsigma\sqrt{2\pi}} \exp\left[ -\frac{\left( \delta_F - \frac{w_t}{N_t(1-\gamma)} \right)^2}{2\varsigma^2} \right] \quad (8)$$

where $\overline{w}_f$ is the mean value and $\varsigma$ the standard deviation. The $j^{th}$ load ranking is obviously independent to the $i^{th}$ strength ranking. To facilitate the understanding and interpretation, this load distribution can then implicitly be converted in stress, assuming the $N_0$ fibers have a constant cross section ($\overline{S}_f$). From this point of view, the average stress applied to fibers corresponds to the stress on tow ($\sigma_{app.t(\gamma)}$) with $\varsigma / \overline{S}_f$ as standard deviation. Of note, structure parameters ($\gamma$ and $\varsigma$) are strongly dependent on manufacturing, weaving and preparation method. They also differ for each sample. The decision was taken to associate a Weibull statistical distributions to them:

$$\varsigma = \varsigma_0 \ln\left(\frac{1}{1-P_\varsigma}\right)^{\frac{1}{m_\varsigma}} \tag{9}$$

$$\gamma = \gamma_0 \ln\left(\frac{1}{1-P_\gamma}\right)^{\frac{1}{m_\gamma}} \tag{10}$$

Where $P_\varsigma$ and $P_\gamma$ are the probabilities of $\varsigma$ and $\gamma$ for a given tow, $m_\varsigma$ and $\varsigma_0$ or $m_\gamma$ and $\gamma_0$ are the Weibull statistical parameters.

### 3.2 Slow crack growth in fibers and tows

The delayed failure of a filament under subcritical stress is assumed to originate from the progressive growth (chemical attack of strained bonds at crack tip) of the critical crack until its threshold size. The convenient Paris-Erdogan law was considered in this work:

$$v = \frac{da}{dt} = V^* \left(\frac{K_I}{K_{IC}}\right)^n = A_1 K_I^n \tag{11}$$

relating the crack velocity ($v$) to stress intensity factor ($K_I$) by a power law. $V^*$ is an environmental constant, $n$ the SCG susceptibility factor, here referred as stress exponent, and $K_{IC}$ the toughness, inferred from the fracture mechanics law:

$$K_I = \sigma_{app} Y \sqrt{a} \tag{12}$$

where $a$ is the crack length and $Y$ the crack geometry factor ($2\,\pi^{-1/2}$ for a penny shaped flaw). Substituting equation (12) into equation (11) and integration from an initial flaw size (strength dependent) to critical size (stress dependent) lead to the developed model as described in [15,16,34,37]:

$$\tau_f = \frac{K_{IC}^{2-n_f}}{A_{1.f}\,\sigma_{app.f}^{n_f} Y^2} \frac{2}{n_f - 2}\left[\sigma_{r.f}^{n_f-2} - \sigma_{app.f}^{n_f-2}\right] \tag{13}$$

where $\tau$ is the time to failure (here the filament one) and $A_1$ an environmental constant ($A_1 = V^* K_{IC}^{-n}$) which evolves with temperature, following an Arrhenius type law:

$$A_1 = A_{10} e^{\frac{-Ea_\tau}{RT}} \quad (14)$$

with T the temperature, $A_{10}$ a material constant, R = 8.314 J $K^{-1}$ $mol^{-1}$ and $Ea_\tau$ the apparent activation energy for SCG.

The delayed failure of a multifilament tow ($\tau_{.t}$) under constant force, based on the bundle theory presented above, can be simplified by failure of the critical fiber with probability $\alpha_t$ which stems from Eq. (15) [44].

$$\alpha_t = 1 - e^{\left(-\frac{n_f - 2}{n_f m_f}\right)} \quad (15)$$

The strength of this critical fiber can be deduced from the Weibull distribution (Eq. (5)). Substituted into equation (13) the following formulation arises:

$$\tau_t = \frac{K_{IC}^{2-n}}{A_{1.t} Y^2 \sigma_{app.t}^n} \frac{2}{n-2} \left[ \left[ \sigma_{1.f}^{n-2} \ln\left(\frac{1}{1-\alpha_t}\right) \right]^{\frac{n-2}{m_f}} - \sigma_{app.t}^{n-2} \right] \quad (16)$$

Expression 16 was however demonstrated to underestimate the variability of $\tau_t$ [34]. In a recent communication, we proposed an adaptation of the model considering not only the flaw size distribution, in sum moderately scattered accounting for a given failure probability $\alpha_t$, but the stress dispersion within the tow as well. Prediction model could hence be described by:

$$\tau_t = \frac{2K_{IC}^{2-n_f}}{(n_f - 2) A_{1.f} Y^2 \sigma_{app.f(P_p)}^{n_f}} \left[ \sigma_{r.f(P_q)}^{n_f - 2} - \sigma_{app.f(P_p)}^{n_f - 2} \right] \quad (17)$$

where $\sigma_{r.f(Pq)}$ and $\sigma_{app(Pp)}$ are respectively the strength (of probability $P_q$ Eq. (5)) and the applied stress (of probability $P_p$ Eq. (8) with $\varsigma$ and $\gamma$ respectively inferred from Eqs. (9) and (10)) of the critical fiber (rank $\alpha_t$ of lifetime in ascending order) piloting the yarn failure. The algorithm did not integrate the load sharing effect, after the results presented in [35] showing its marginal and null impacts on lifetime variability and scale effect respectively. Implicitly,

this formulation marks a breakthrough in interpretation of bundle failure under static fatigue conditions as the lifetime can no longer be associated to fiber strength distributions, as done on filament by [22]. An intermediate time to failure can indeed equivalently result from a strong and overloaded critical fiber, or vice versa, from a weak underloaded filament, all being ruled by the weakest link theory. Of note, this expression uses the filament SCG parameters: $n_f$ and $A_{1.f}$. Never assessed by static fatigue on filaments other than Hi-Nicalon, this work proposes to use the tow lifetime [16,48] to estimate them.

### 3.3 Monte Carlo simulation tool

The Monte Carlo algorithm used to simulate the tow lifetime was presented in previous works [26,35]. It is based on the belief stress inhomogeneity plays a critical role on time to failure variability and SCG parameters assessment. Indeed, the stress on tow, as well as the load distribution and the stress applied to the critical fiber, are unknown for a static fatigue probe. The developed algorithm is divided in 3 steps: (i). assignment of bundle structure, (ii). assignment to each fiber of a stress and a strength, (iii). calculation of fiber time to failure used to assess the virtual tow lifetime. For the 2 first steps, random numerical values ($P_\gamma$, $P_\varsigma$, $P_i$ and $P_j$) were selected, independently from each others. Equation 13 was used for the third step, individual filament lifetimes finally ranked to define bundle virtual lifetime (corresponding to filament of rank $\alpha_t$). The stochastic character of this operation (each tow has a unique architecture) was used to identify the lifetime variability. The above scheme was repeated 1000 times for each $w_t$ (100-1400 MPa $\sigma_{app.t}$ range). This algorithm can be reverse operated by adjusting empirically $n_f$ and $A_{1.f}$ coefficients to fit the median tow behavior.

# 4. Results and discussion

### 4.1 Tensile tests on filaments and tows

Mechanical properties for the 8 types of filaments, extended to 9 considering the 2 TS batches, are first presented. Tensile strengths exceeding 2000 MPa were experimentally measured on these fibers, with Young moduli ranging from 180 to 220 GPa on first-generation, close to 300 GPa on the second-generation and above 400 GPa on the third-generation. Toughness, extracted from fractographic analysis [31,49], ranges from 1 to 1.2 MPa $m^{1/2}$ when silicon oxycarbide phase is present on first-generation fibers and lies >1.5 MPa $m^{1/2}$ when absent [50]. Weibull moduli ranging from 4.3 to 10, were estimated by linear regression ($\ln(\sigma_{r,f})$ versus $\ln(-\ln(1-P_i))$) (Table 2). TS11 shows lower and more scattered tensile strength compared to TS which, together with Hi-Ni and Hi-Ni-S, display the highest Weibull modulus.

| Fiber | Number of test | $\sigma_{r,f}$ ± std. dev. (MPa) | $\varepsilon_{f,f}$ (%) | $E_f$ (GPa) | $m_f$ | $\sigma_{1,f}$ (MPa) | $K_{IC}$ (MPa $m^{1/2}$) |
|---|---|---|---|---|---|---|---|
| NL207 | 100 | 2839 ± 667 | 1.3 | 210 | 5.05 | 3090 | 1.20 |
| TS | 100 | 3152 ± 624 | 1.8 | 180 | 8.17 | 3550 | 1.11 |
| TS11 | 40 | 2776 ± 647 | 1.5 | 180 | 4.79 | 3034 | 1.12 |
| Lox-M | 44 | 2984 ± 695 | 1.5 | 200 | 4.63 | 3314 | 1.11 |
| ZMI | 49 | 3076 ± 742 | 1.5 | 200 | 4.81 | 3372 | 1.01 |
| Hi-Ni | 49 | 3136 ± 368 | 1.0 | 300 | 9.84 | 3295 | 1.66 |
| Hi-Ni-S | 44 | 2877 ± 414 | 0.7 | 410 | 8.42 | 3062 | 1.86 |
| NL101 | 50 | 2166 ± 559 | 1.2 | 180 | 4.28 | 2390 | 1.20 |
| AM | 92 | 2815 ± 533 | 1.6 | 180 | 5.74 | 3024 | 1.20 |

**Table 2**: Mechanical properties of SiC-based fibers.

Mechanical properties of multifilament tows are presented in table 3. As expected from the bundle theory, tensile strength lies below the filament one (<2000 MPa). The lowest values were measured on NL207, NL101 and AM types ($\sigma_{r,t}$<1000 MPa) and the highest on Hi-Nicalon-S. Structural parameters, assessed from curvature in the 0-30 N range (re-loading *cf.*

theory section), are gathered in Table 4. The mean fraction of unloaded section ($\bar{\gamma}$) extends from 10 to 25% for TS11 and Hi-Ni-S or Lox-M respectively. It is worth noting negative $\gamma$ values could, in some cases, be extracted from bundle tensile test meaning a Young modulus on tow exceeding the fiber one (Eq. (4)). Two approximations can explain such non-intuitive result: either the over-estimation of filament Young modulus which shows some variation, or the under-estimation of bundle section (Eq. (3) based on weight and density) evaluated on a 300 mm long sample whereas only 25 mm gauge length specimens were effectively tested. This latter argument is the most pertinent. Weibull moduli describing the variability of $\gamma$ are close to each others, extending from 1.3 to 2.5 [48]. The fiber slack $\varsigma$ extends in average from 0.01 to 0.04 N, respectively on TS and Hi-Ni-S. This parameter, apparently independent to $\gamma$, seems to increase with fiber diameter or to decrease when $N_t$ increases (Table 1): <0.025 N for diameters < 12µm or > 500 filaments per tow and vice versa. The lowest value is found with TS containing 1600 filaments in each tow. The Weibull modulus on this coefficient extends from 3.5 to 7.

| | Number of tests | $\sigma_{f.t(\bar{\gamma})}$ (MPa) | $F_{f.t}$ (N) | $\varepsilon_{f.t}$ (%) |
|---|---|---|---|---|
| NL207 | 30 | 750 | 57 | 0.60 |
| TS | 100 | 1300 | 100 | 1.10 |
| TS11 | 30 | 1100 | 87 | 0.98 |
| Lox-M | 30 | 1400 | 95 | 1.00 |
| ZMI | 30 | 1350 | 110 | 0.90 |
| Hi-Ni | 30 | 1800 | 120 | 0.93 |
| Hi-Ni-S | 26 | 1600 | 82 | 0.80 |
| NL101 | 30 | 870 | 57 | 0.84 |
| AM | 30 | 810 | 60 | 0.71 |

**Table 3**: Mechanical properties of SiC-based multifilament tows.

| $\bar{\gamma}$ ± std. | Me(γ) | $\gamma_{min}$ / $\gamma_{max}$ | $m_\gamma$ | $\gamma_0$ | $\bar{\varsigma}$ | Me(ς) | $m_\varsigma$ | $\varsigma_0$ |
|---|---|---|---|---|---|---|---|---|

| | dev. (%) | (%) | (%) | | (%) | (N) | (N) | | (N) |
|---|---|---|---|---|---|---|---|---|---|
| NL207 | 11 ± 9.0 | 11.1 | -11 / 29.5 | 2.44 | 28.9* | 0.0268 | 0.0259 | 6.86 | 0.0273 |
| TS | 16 ± 11.2 | 14.3 | 0 / 44.0 | 1.45 | 18.3 | 0.0099 | 0.0089 | 4.29 | 0.0097 |
| TS11 | 10 ± 8.5 | 10.7 | 0 / 33.1 | 1.31 | 11.8 | 0.0179 | 0.0175 | 5.96 | 0.0186 |
| Lox-M | 25 ± 8.1 | 22.1 | 12.5 / 38.6 | 1.38 | 15.5* | 0.0240 | 0.0228 | 5.84 | 0.0243 |
| ZMI | 14 ± 8.5 | 14.1 | -3 / 27.9 | 2.26 | 16.6* | 0.0211 | 0.0202 | 5.29 | 0.0216 |
| Hi-Ni | 14 ± 12 | 14.3 | -9 / 39.6 | 2.16 | 27.3* | 0.0259 | 0.0260 | 6.93 | 0.0274 |
| Hi-Ni-S | 25 ± 16 | 21.2 | 0 / 53.4 | 1.43 | 29.0 | 0.0406 | 0.0399 | 3.53 | 0.0443 |
| NL101 | 15 ± 13 | 14.3 | -13 / 58 | 1.50 | 32.9* | 0.0285 | 0.0262 | 5.39 | 0.0311 |
| AM | 13 ± 11 | 13.1 | -5.0 / 46 | 2.14 | 26.3* | 0.0180 | 0.0171 | 5.54 | 0.0195 |

**Table 4**: Structural parameters of multifilament tows assessed by tensile testing. * indicate the dataset was offsetted to define the distribution as per [48].

### 4.2 Delayed failure under static fatigue conditions

Static fatigue data at different temperatures were presented in a previous work [48]. The power law was found to satisfactorily fit the median time to failure, illustrated by endurance diagrams ($\ln(\sigma_{app.t}(\bar{\gamma}_t)) - \ln(\tau_t)$) (Fig. 1a). Table 5 gathers the SCG parameters extracted this way on each fiber type. $n_t$ ranges from 4.9 on Lox-M to 9.1 on ZMI. $A_{1.t}$ coefficients cover several orders of magnitude, result strongly dependent on the stress exponent or fiber toughness (Table 2). For instance, Hi-Ni-S and ZMI at 600 °C display similar lifetimes [25] but clearly different $A_{1.t}$ values ($1.4 \times 10^{-12}$ *vs*. $2.6 \times 10^{-9}$ $m^{1-n/2}$ $MPa^{-n}$ $s^{-1}$ respectively). Alternatively, $V^*$ (Eq. 11) constant can be used ($1.2 \times 10^{-10}$ *vs*. $2.9 \times 10^{-9}$ m $s^{-1}$ at 600 °C for Hi-Ni-S and ZMI) showing closer values. The apparent activation energy for SCG, which could be indicative of different chemical reaction responsible for crack growth, ranges from 100 to 200 kJ $mol^{-1}$, higher on ZMI, Hi-Ni and Hi-Ni-S and lower for TS and TS11. NL207 and Lox-M are intermediate.

| | NL207 | TS | TS11 | Lox-M | ZMI | Hi-Ni | Hi-Ni-S |
|---|---|---|---|---|---|---|---|

| $n_t$ | 7.3 | 5.0 | 5.8 | 4.9 | 9.1 | 8.4 | 7.2 |
|---|---|---|---|---|---|---|---|
| T (°C) | $A_{1.t}$ ($m^{1-n/2}$ $MPa^{-n}$ $s^{-1}$) × $10^{-12}$ | | | | | | |
| 400 | - | $3.28^{[2;6]}$ | - | $0.149^{[1;2]}$ | $1.57^{[1;2]}$ | - | - |
| 450 | $4.62^{[1;3]}$ | $8.21^{[7;46]}$ | $2.36^{[2;10]}$ | $0.893^{[3;9]}$ | $7.85^{[4;9]}$ | - | - |
| 500 | $11.6^{[3;5]}$ | $17.3^{[4;34]}$ | $11.8^{[4;24]}$ | $2.23^{[3,23]}$ | $52.4^{[3;17]}$ | $29.6^{[8;79]}$ | $0.0618^{[1;2]}$ |
| 550 | $116^{[5;47]}$ | $38.6^{[5;65]}$ | $31.5^{[4;34]}$ | $8.93^{[6;40]}$ | $262^{[4;58]}$ | - | - |
| 600 | $154^{[2;22]}$ | $109^{[5;51]}$ | $47.3^{[4;44]}$ | $99.2^{[4;34]}$ | $2620^{[6;111]}$ | $1480^{[6;17]}$ | $1.41^{[7;19]}$ |
| 650 | $308^{[6;99]}$ | $821^{[8;280]}$ | $236^{[6;70]}$ | $446^{[8;9]}$ | $22400^{[5;44]}$ | - | - |
| 700 | - | - | - | - | - | $18500^{[3;5]}$ | $17.6^{[3;3]}$ |
| 750 | $4620^{[6;86]}$ | $1310^{[5;46]}$ | $473^{[2;22]}$ | $1790^{[4;22]}$ | $52400^{[7;46]}$ | - | - |
| 800 | - | - | - | - | - | $148000^{[5;17]}$ | $131^{[9;14]}$ |
| 850 | $15400^{[4;29]}$ | $3280^{[3:19]}$ | $945^{[2;10]}$ | $1790^{[2;9]}$ | $131000^{[4;17]}$ | - | - |
| 900 | - | - | - | - | - | $847000^{[5;43]}$ | - |
| $Ea_{\tau.t}$ (kJ $mol^{-1}$) | 139 | 98 | 100 | 146 | 172 | 192 | 176 |
| $A_{10.t}$ ($m^{1-n/2}$ $MPa^{-n}$ $s^{-1}$) | $4.19 \times 10^{-2}$ | $1.13 \times 10^{-4}$ | $6.63 \times 10^{-5}$ | $2.96 \times 10^{-2}$ | 31.0 | 325 | $5.04 \times 10^{-2}$ |

**Table 5**: SCG coefficients (Eq. (13)), estimated on SiC-based tows under static fatigue conditions at constant force and various temperatures. Exponents in brackets [x;y] indicate: x the number of tested stresses and y the total number of tests performed at each temperature.

Similarly to filament strength, the bundle lifetime variability can nicely be described using the Weibull statistic (Fig. 1b) [38,51,52]:

$$P_\tau = 1 - e^{-\left(\frac{\tau_t}{\tau_{t0}}\right)^{m_{\tau t}}} \quad (18)$$

where $P_\tau$ is the lifetime probability, $\tau_t$ is the tow lifetime, $\tau_{t0}$ the characteristic time to failure and $m_{\tau t}$ the static fatigue Weibull modulus. Moduli ranging from 0.5 to 1.9 (>1 on sized Tyranno® and <1 for Nicalon®) were calculated on the different fibers at different conditions (Table 6). The consistency of this modulus for various temperatures and applied stresses further indicates this value can be considered as constant for a given fiber type, result of prime interest for Strength-Probability-Time diagram construction [53] that would assist the composite engineering. This value is however pertinent to the testing setup and sample preparation method.

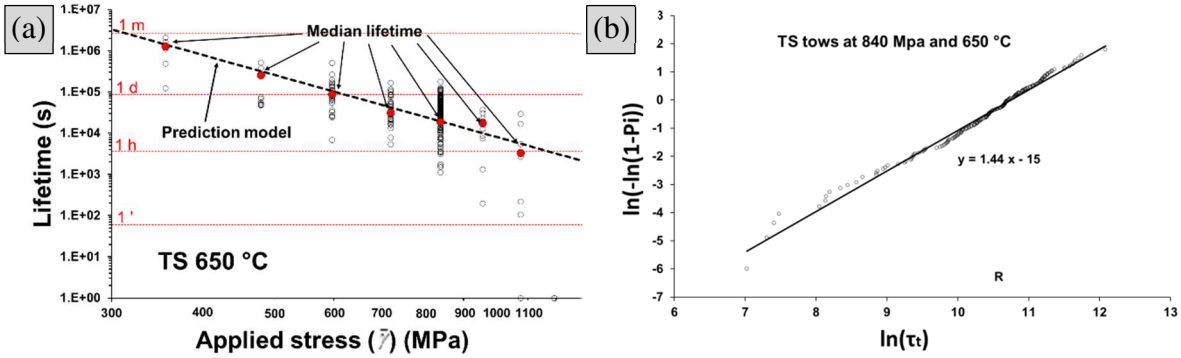


**Fig. 1**: (a). Endurance diagram for TS tows static fatigue data under ambient air at 650 °C and (b). $\tau_t$ distribution under $\sigma_{app.t(\bar{\gamma})}$ = 840 MPa. Two hundreds (200) tests were conducted in this particular condition, to sustain the statistical approach.

| Fiber | Condition | $m_{\tau t}$ | $\tau_{t0}$ (s) | Reference |
|---|---|---|---|---|
| NL207 | 850 MPa 650 °C | 0.67 | $1.02 \times 10^5$ | |
| TS | 955 MPa 500 °C | 1.46 | $5.88 \times 10^5$ | |
| TS | 717 MPa 550 °C | 1.49 | $1.23 \times 10^6$ | |
| TS | 840 MPa 550 °C | 1.44 | $6.05 \times 10^5$ | |
| TS | 955 MPa 550 °C | 1.45 | $2.40 \times 10^5$ | |
| TS | 355 MPa 650 °C | 1.44 | $1.32 \times 10^6$ | |
| TS | 600 MPa 650 °C | 1.45 | $1.20 \times 10^5$ | |
| TS | 717 MPa 650 °C | 1.47 | $4.94 \times 10^4$ | |
| TS | 840 MPa 650 °C | 1.44 | $4.67 \times 10^4$ | |
| TS11 | 830 MPa 650 °C | 1.83 | $3.50 \times 10^4$ | |
| Lox-M | 940 MPa 650 °C | 1.30 | $2.66 \times 10^4$ | |
| ZMI | 810 MPa 650 °C | 1.30 | $5.45 \times 10^5$ | |
| Hi-Ni | 1160 MPa 500 °C | 0.91 | $1.50 \times 10^5$ | [23] |
| Hi-Ni | 1740 MPa 500 °C | 0.53 | $2.04 \times 10^4$ | [23] |
| Hi-Ni | 350 MPa 900 °C | 0.45 | $2.66 \times 10^5$ | [23] |
| Hi-Ni-S | 1300 MPa 600 °C | 0.78 | $2.06 \times 10^5$ | [54] |

**Table 6**: Distribution of SiC-based tows static fatigue experimental data at various conditions, temperature or applied stress ($\sigma_{app.t(\bar{\gamma})}$), interpreted by Weibull statistic.

### 4.3 Evaluation of filament SCG coefficients

The algorithm used to simulate the time to failure of a tow from the filament properties and structural parameters was described in theory section. It was reverse operated in the present work to estimate the filament parameters. Fiber strength and stress were randomly selected

from the established distributions above given. It is worth reminding the stress was extracted from a normal distribution, with a γ-dependent mean value and a standard deviation themselves randomly and independently selected. The filament SCG coefficients ($A_{1.f}$ and $n_f$) were empirically defined, prior to run sets of simulations: 1000 tows computed for each $\sigma_{app.t}$ ranging from 100 to 1400 MPa (100 MPa steps). The median lifetime at each stress was then used to construct the endurance diagram and extract the virtual tow lifetime prediction parameters ($A_t$ or $A_{1.t}$ and $n_t$). These values were finally compared to experimental data (Table 5) and the process repeated until appropriate parameters were identified. Endurance diagrams are presented in *supplementary document S.1*.

On NL207 for instance, with $n_f = 7.3$ simulation led to $n_t = 5.3$ highlighting the scale effect. The approach here consisted to cover the 5 to 15 $n_f$ range and deduce its relationship to $n_t$. On the same example, with $n_f = 5$, 10 and 15, respective $n_t = 3.6$, 7.3 and 11 were calculated from the virtual sets. Of note, in the context of this algorithm $n_f$ and $n_t$ were found to be linearly related (Fig. 2a), with a slope and an ordinate pertinent to the structure. On NL207, this process ends-up defining $n_f = 10$ (desired $n_t = 7.3$) and $A_{1.f} = 1.3 \times 10^{-9}$ $m^{1-n/2}$ $MPa^{-n}$ $s^{-1}$ at 650 °C. Repeated with other fiber types, the same linearity was noticed (Fig. 2) helping to identify the following filament stress exponents: 7.4, 8.2, 7.3, 13.6 and 13.8 respectively for TS, TS11, Lox-M, ZMI and Hi-Ni-S (Table 7). The same value for Hi-Ni was reported in a previous work: 12.6 [22,26] confirmed by experimental works. These stress exponents are structure-independent (unlike $n_t$) and thought to be intrinsic to the fiber type (microstructure and chemical composition). This will be discussed afterward.

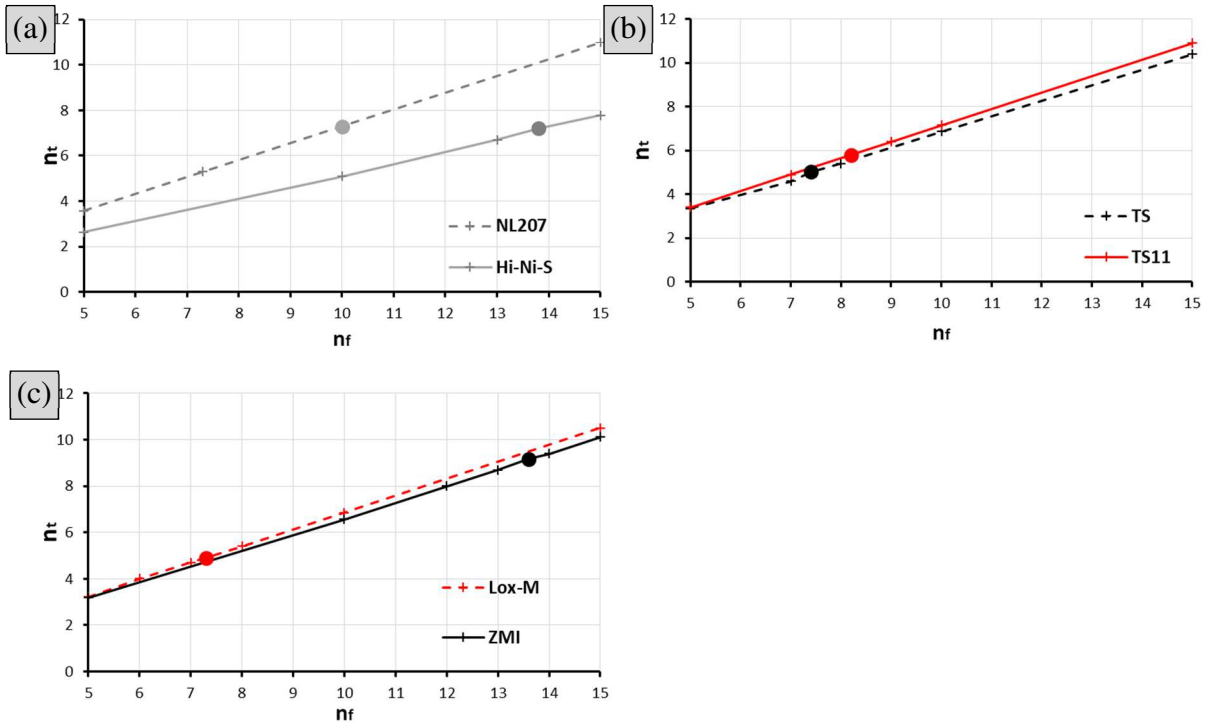


**Fig. 2**: Evolution of simulated $n_t$ with $n_f$ for (a). Hi-Ni-S and NL207, (b). TS and TS11, (c). Lox-M and ZMI. Dots identify the right $n_f$ value leading to experimentally assessed $n_t$. Critical $\alpha_t$ fraction was adjusted to $n = n_f$ (Eq. (15)).

| Fiber | NL207 | TS | TS11 | Lox-M | ZMI | Hi-Ni | Hi-Ni-S |
|---|---|---|---|---|---|---|---|
| $n_f$ | 10.0 | 7.4 | 8.2 | 7.3 | 13.6 | 12.6 | 13.8 |
| $\alpha_t$ (%) | 14.7 | 8.54 | 14.6 | 14.5 | 16.2 | 8.19 | 9.66 |
| Temperature | $A_{1.f}$ ($m^{1-n/2}$ $MPa^{-n}$ $s^{-1}$) × $10^{-12}$ | | | | | | |
| 400 °C | - | 11 | - | 0.23 | 9.5 | - | - |
| 450 °C | 8.0 | 30 | 7.0 | 1.5 | 100 | - | - |
| 500 °C | 25 | 55 | 32 | 4.5 | 350 | 10 | 0.01 |
| 550 °C | 300 | 130 | 110 | 22 | 2500 | | |
| 600 °C | 440 | 400 | 150 | 250 | 45000 | 330 | 0.3 |
| 650 °C | 1300 | 1500 | 1400 | 500 | 500000 | - | - |
| 700 °C | - | - | - | - | - | 6000 | 3.4 |
| 750 °C | 12000 | 4400 | 1700 | 4000 | 1100000 | - | |
| 800 °C | - | - | - | - | - | 65000 | 18 |
| 850 °C | 70000 | 8000 | 3500 | 4000 | 4500000 | - | - |
| 900 °C | - | - | - | - | - | 160000 | - |
| Ea (kJ $mol^{-1}$) | 153 | 98.3 | 107 | 149 | 194 | 188 | 173 |
| $A_{10.f}$ ( $m^{1-n/2}$ $MPa^{-n}$ $s^{-1}$) | 0.76 | $3.4 \times 10^{-4}$ | $5.3 \times 10^{-4}$ | $9.0 \times 10^{-2}$ | $1.0 \times 10^{4}$ | 64 | $5.8 \times 10^{-3}$ |

**Table 7**: Slow crack growth parameters describing the median lifetime of SiC-based filaments at various intermediate temperatures, estimated by Monte Carlo simulation fitting experimental lifetime data obtained on multifilament scale.

The stress exponent ranking is almost unchanged for filaments or tows (Table 5): Lox-M and TS show the lowest values (7.3 and 7.4 respectively) TS11 and NL207 are intermediate (8.2 and 10) whereas Hi-Ni, Hi-Ni-S and ZMI are close to 13 (12.6, 13.8 and 13.6 respectively). The main observation concerns the Hi-Ni-S, which was close to NL207 at bundle scale and ends up being the largest at filament scale with $n_f$ = 13.8. The scale effect on stress exponent (here referring to the mismatch $n_f$-$n_t$) was observed in all cases, more or less pronounced. It is similar on NL207, TS, TS11, Lox-M and close to 2.5, larger on Hi-Ni and ZMI with 4.5 whereas it reaches 6.6 on Hi-Ni-S, to be linked to the particularly degraded structure of this latter type (Table 8). In a previous study [35], we interpreted this scale effect by the fact stress to the critical filament is larger than its mean value (stress to tow), however used to construct the endurance diagram and calculate $n_t$. Globally, low $\alpha_t$ (lower critical rank) and high $\varsigma$ exacerbate this scale effect.

| | $m_f$ | Me($\varsigma$) | $m_\varsigma$ | $\alpha_t$ | $n_f$ | $n_t$ | $n_f$-$n_t$ |
|---|---|---|---|---|---|---|---|
| NL207 | 5.05 | 0.0259 | 6.86 | 14.7 | 10 | 7.3 | 2.7 |
| TS | 8.17 | 0.0089 | 4.29 | 8.54 | 7.4 | 5 | 2.4 |
| TS11 | 4.79 | 0.0175 | 5.96 | 14.6 | 8.2 | 5.8 | 2.4 |
| Lox-M | 4.63 | 0.0228 | 5.84 | 14.5 | 7.3 | 4.9 | 2.4 |
| ZMI | 4.81 | 0.0202 | 5.29 | 16.2 | 13.6 | 9.1 | 4.5 |
| Hi-Ni | 9.84 | 0.0260 | 6.93 | 8.19 | 12.6 | 8.4 | 4.2 |
| Hi-Ni-S | 8.42 | 0.0399 | 3.53 | 9.66 | 13.8 | 7.2 | 6.6 |

**Table 8**: Summary of filament and tows stress exponents for the different SiC-based fibers, with the parameters impacting it.

Finally, $A_{1.f}$ coefficients, estimated for each tested temperatures are gathered in Table 7. Despite higher stress exponents, $A_{1.f}$ coefficients are not drastically higher than $A_{1.t}$ (less than 100 times higher). Their evolution with temperature was used to calculate an apparent slow crack growth activation energy, close to the tow ones. No scale effect on this energy is hence

highlighted by the simulation (if existing not structure related), despite literature data indicating it on Hi-Ni (188 kJ $mol^{-1}$ [15] for tow against 147 kJ $mol^{-1}$ on filaments [22]).

Above results focused on the median times to failures. Their scatter is now reviewed. The variability of experimental and computed times to failure results were first compared in one condition extensively tested. The range of virtual lifetime was found to convincingly encompass experimental datasets (Fig. 3). Some discrepancies between calculated and computed $m_{\tau t}$ moduli can be noticed comparing tables 6 and 9. The exactitude of the former modulus, extracted from 30 tests only, can however be questioned as mentioned in [38]. Nonetheless, some coherency should be highlighted: moduli respectively below and above 1.0 on Nicalon® and Tyranno®. Hi-Ni-S combines the highest $n_f$ value with the worst bundle structure, its $m_{\tau t}$ modulus is thus, and with no surprise, the lowest. The consistency of this Weibull distribution over the applied stress range is shown in the *supplementary document S.1*.

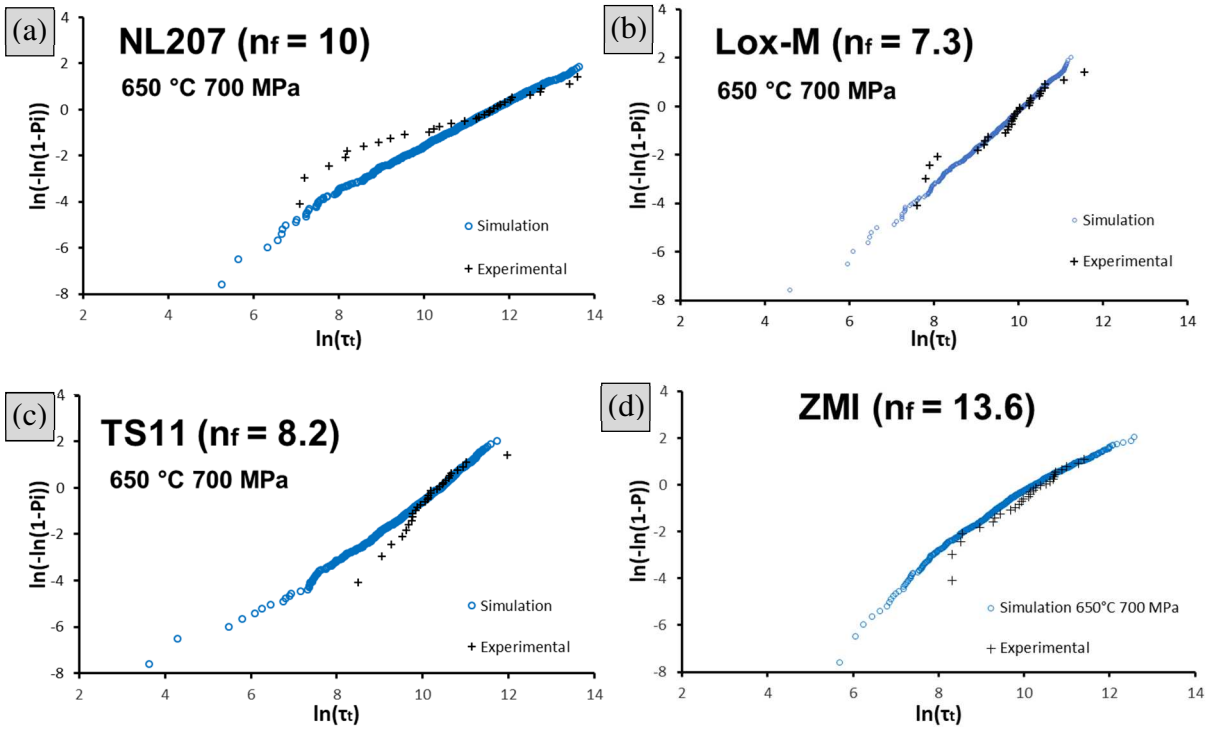


**Fig. 3**: Weibull diagrams comparing experimental and simulation data at 650 °C and $\sigma_{app.t(\gamma = 0\%)}$ = 700 MPa on (a). NL207, (b). TS11, (c). Lox-M and (d). ZMI, with slow crack growth parameters attributed to filaments given in table 7.

| | $n_t$ | $n_t$ (lower) | $n_t$ (upper) | $m_{\tau t}$ |
|---|---|---|---|---|
| NL207 | 7.3 | 7.5 | 8.1 | 1.00 |
| TS | 5.0 | 5.5 | 6.6 | 1.15 |
| TS11 | 5.8 | 6.6 | 7.1 | 1.30 |
| Lox-M | 4.9 | 5.5 | 6.3 | 1.45 |
| ZMI | 9.1 | 8.4 | 12 | 1.14 |
| Hi-Ni | 8.4 | 10 | 9.5 | 0.75 |
| Hi-Ni-S | 7.2 | 7.8 | 12 | 0.38 |

**Table 9**: Parameters describing the distribution of virtual lifetimes, independent to the temperature.

Figure 4 shows the endurance diagrams as extracted from simulations, compared to experimental data points at various stresses and one temperature. Results confirm the comfortable encompassment of test data for all applied stresses. It is worth noting, as mentioned above, $A_{1.f}$ input coefficient was not adjusted to suit the upper lifetime range, as alternatively proposed elsewhere [34,44], but its median values. It is thus remarkable to note lower, but also upper lifetimes could be simulated. This comforts the selected approach.

These diagrams highlight a second finding of the algorithm: fact the median lifetime is not logarithmically centered between lower and upper bonds (delimited by extremely favorable or unfavorable structural configurations). This is explained by respective prevailing weights of $\varsigma$ and $\gamma$ at low and high stresses, discussed in a previous study [35] (see *supplementary document S.2*). These limits can as well be described by a power law, with higher stress exponents (Table 9). In any case, lower limit of simulated lifetime appears to be more critical than experimentally observed, and sharply falls to zero around 900-1000 MPa, or 700 MPa for Hi-Ni-S, in the 600-650 °C range. At higher temperature, this value further decreases due to accelerated SCG mechanism as shown in the *supplementary document S.3*.

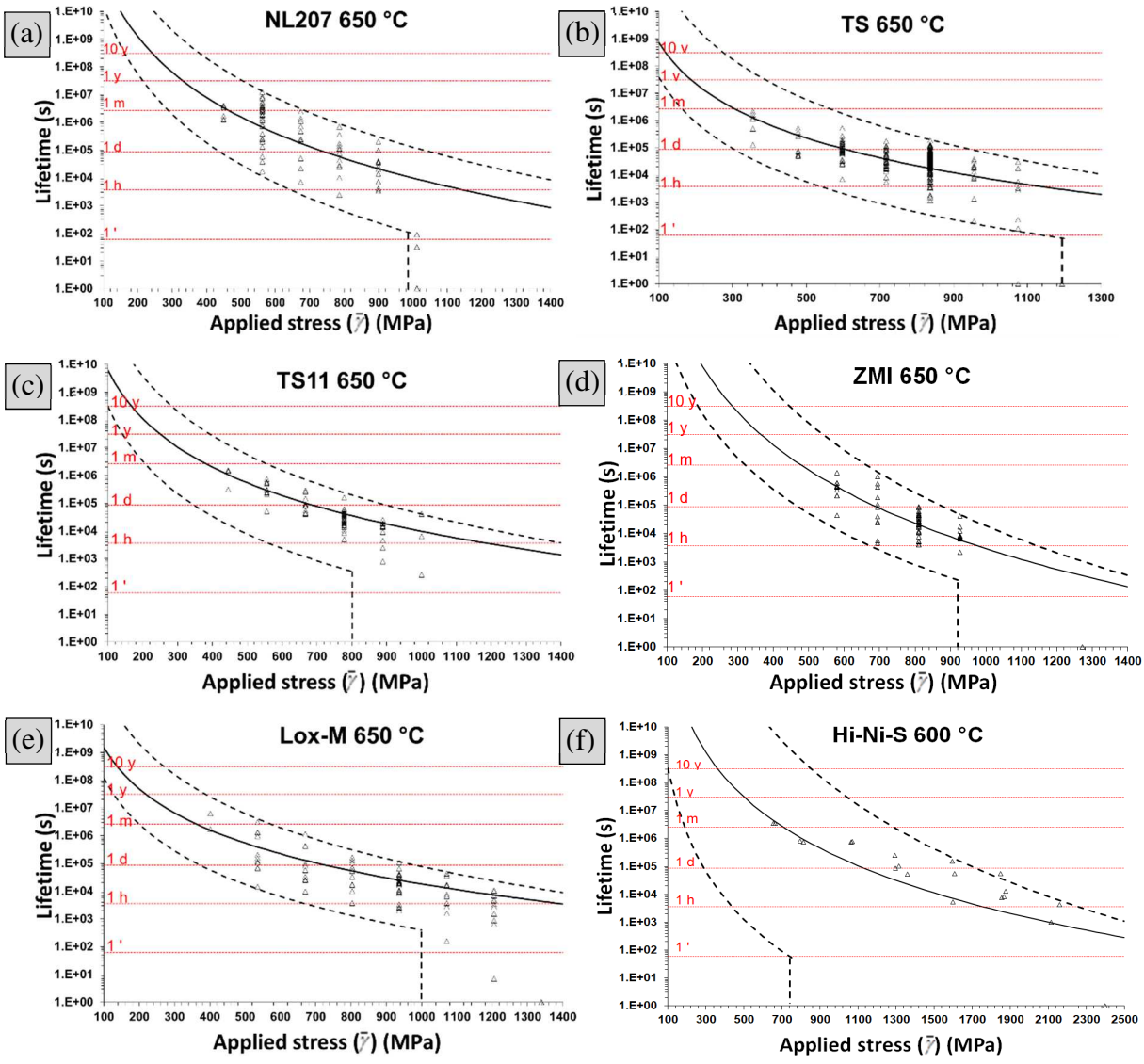

**Fig. 4**: Comparison, on time to failure-stress diagrams, of experimental and simulation-deduced lifetime scatter for (a). NL207 (b). TS, (c). TS11, (d). ZMI, (e). Lox-M at 650 °C and (f). Hi-Ni-S at 600 °C. Simulations were performed using parameters given in Table 7 for filament slow crack growth and Table 4 for structural parameters.

### 4.4 Lifetime prediction: type to type comparison

Selection for a fiber type over the others must fulfil a complex list of requirements, subject we do not aim to exhaustively review. Manufacturing process and application conditions, including their versatility, are obviously the pillars for such argumentation. Sensitivity to SCG, thermo-mechanical and chemical properties of the reinforcement [55] are, as a matter of fact, of prime importance. Nonetheless Hi-Ni and Hi-Ni-S are the only candidate for high temperature application (>1000 °C) given their thermal stability, no restriction exists for intermediate duty usage (<1000 °C). Therefore, endurance diagrams presenting median predicted lifetime for filaments or tows at various temperatures types are given in Figure 5.

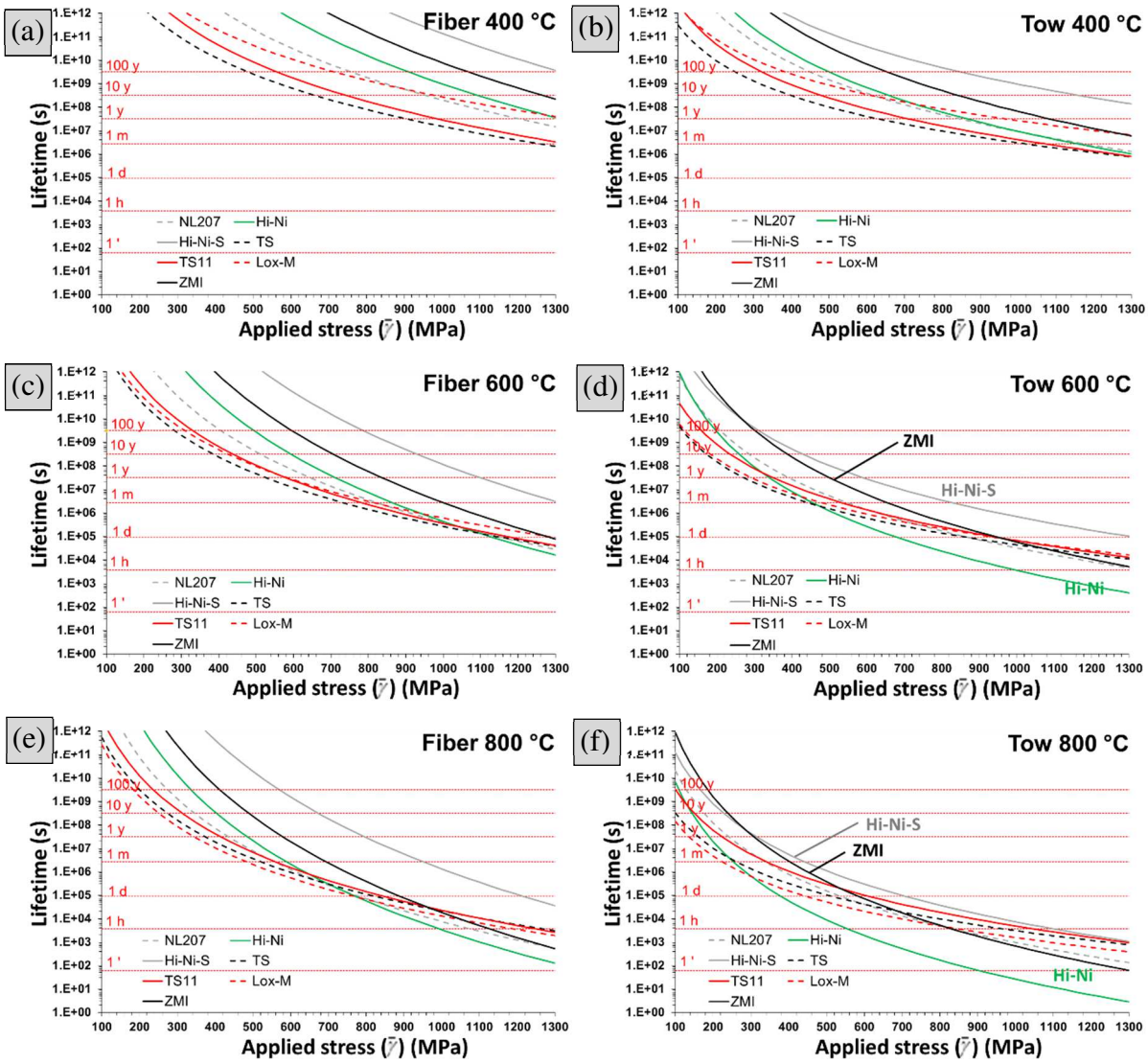


**Fig. 5**: Endurance diagrams comparing the different filaments or tows types (median lifetime) at (a-b). 400 °C (c-d). 600 °C or (e-f). 800 °C, considering Arrhenius estimated $A_{1.t}$ and $A_{1.f}$ coefficients.

Filaments display a significantly longer time to failure, as expected after the bundle theory (tow ruin piloted by weak filaments). The practical consequence is the requirement to test single fibers at high stress and temperature to reach a comfortable test duration with associated drawbacks such as loading failure or application representativity. Despite a scale effect varying from type to type as above mentioned (Table 8), the lifetime ranking for filaments or bundles is identical: ZMI and Hi-Ni-S display longer times to failure whereas TS,

TS11, Lox-M are close to each others (Fig. 5). It becomes worth promoting the Hi-Ni type for temperatures for temperatures below 600°°C and low applied stresses. Based on these results, ZMI would be preferred over Hi-Ni for long service time. Such conclusion, based on median lifetime, however neglect the hierarchical scale effect: bundles are piloted by weakest filaments and composites are piloted by weakest tows [42]. Thus it becomes pertinent to integrate the failure time probability to justify such decision.

A key outlook for these simulations is the capacity to construct SPT diagrams from the 1000 virtual tow lifetimes at each conditions, as proposed in Figure 6a,b at 600 °C for Hi-Ni-S and NL207. Structure-induce lifetime variability is highlighted on Hi-Ni-S: despite high median lifetime (close to 10 times larger than NL207), weakest tows display very short times to failure, lower than NL207. In other words and as a fiber type selection criteria, control of fiber alignment in a bundle can overpass the intrinsic resistance to SCG. Above diagram comparing the median lifetime for the different types of fiber was hence repeated for failure time probabilities of 1% and 10% (Fig. 6c,d). The most promising fiber type, based on this criteria, appears to be the ZMI. All other fibers are close to each others for applied stresses close to 500 MPa. At a low stress, TS and Lox-M are disadvantaged compared to NL207 and Hi-Ni. This result is obviously pertinent to used batches and testing method but illustrates the need to understand and model the bundle structure for composite engineering. Additional SPT and endurance diagrams can be found in the *supplementary document S.4*.

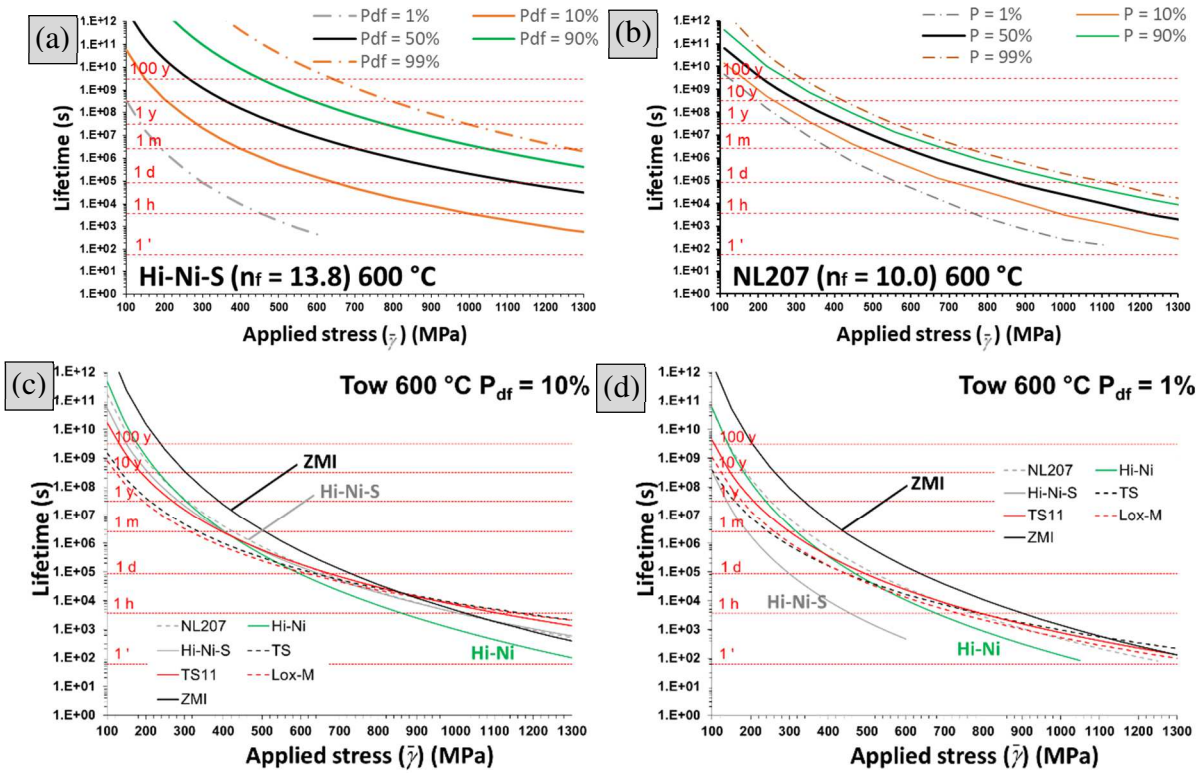


**Fig. 6**: Simulated Stress-Probability-Time to failure diagrams for (a). Hi-Ni-S and (b). NL207 tows at 600 °C. Endurance diagram comparing the bundle time to failure at 600 °C for rupture probabilities of (c). 10% or (d). 1%.

### 4.5 Sensitivity to SCG of SiC-based fibers

Above section has presented the fiber and tow mechanical properties used as an input for the algorithm. Filament stress exponents assessed by this mean range from 7.3 to 13.8 with three apparent groups: (i). TS, TS11 and Lox-M with $n_f$ close to 7.5, (ii). NL207 with $n_f$ = 10 and (iii). ZMI, Hi-Ni and Hi-Ni-S with $n_f$ close to 13. These three groups can almost be found comparing the SCG apparent activation energy: (i). TS and TS11 have $Ea_\tau$ about 100 kJ mol$^{-1}$, (ii). NL207 and Lox-M have $Ea_\tau$ about 150 kJ mol$^{-1}$ and (iii). ZMI, Hi-Ni and Hi-Ni-S have $Ea_\tau$ about 180 kJ mol$^{-1}$ (Fig. 7a). Discrepancy between above families, $n_f$ or $Ea_\tau$ based, could be partly ascribed to disturbing effect of doping elements (present in Tyranno® fibers) [56]. Such effect was evidence in a previous communication using tow parameters [25]: stabilizing effect of zirconium and destabilizing effect of titanium on the amorphous silicon oxicarbide

continuum. The presence of titanium would mostly bias the stress exponent (TS, TS11, Lox-M $n_{f.titanium}$<10). Distinction of the fiber type was hence simplified to two categories:

(i). family REAC for chemically reactive fibers (NL207, TS, TS11, Lox-M);

(ii). family STAB for chemically stable fibers (ZMI, Hi-Ni, Hi-Ni-S).

The former group gathers substrate with high oxygen content (>10 at.%, Table 1), high hydrogen (>6 at.%) and non-stabilized or titanium doped oxycarbide phase. The latter group gathers oxygen-free fibers (second and third generation) or the zirconium stabilized one. Moreover, a relationship between the stress exponent and $V^{*1/n}$ is highlighted on Figure 7d.

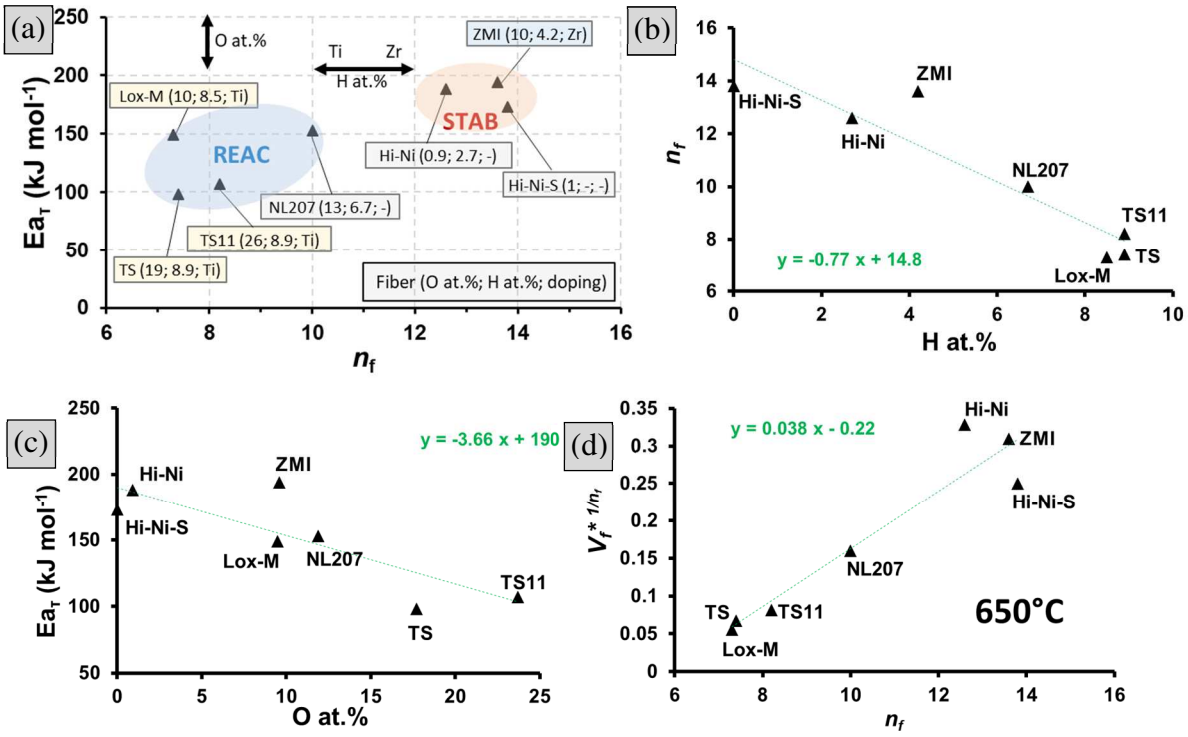


**Fig. 7**: (a). Summary of SiC-based filament SCG parameters compared with their chemical composition. Evolution of (b). filament stress exponent with the hydrogen content, (c). apparent activation energy with the oxygen content and (d). $V^{*1/n}$ with $n_f$.

Based on this latter categorization, $n_f$ larger than 12 would correspond to STAB family (poorly hydrogenated); $n_f$ below or equal 10 be representative of the REAC group. Figures 7b

and 7c illustrate respectively the relationships between $n_f$ and the hydrogen content or between $Ea_\tau$ and the oxygen content. These appear as parameters affecting the sensitivity of theses fibers to slow crack growth mechanism. $Ea_\tau$ of REAC substrates ranges between 100 and 150 kJ $mol^{-1}$ similarly to glass one [57], whereas STAB family display $Ea_\tau$ values above 170 kJ $mol^{-1}$ similarly to carbon oxidation [58] (Table 7). From this statement, following mechanisms could be conjectured:

(i). oxidation of oxycarbide phase strained chemical bonds followed by their hydrolysis (induced by water vapor from environment or in-situ hydrogen content) for REAC fibers;

(ii). oxidation of percolated carbon free network [59] for STAB fibers.

Indeed, these latter fibers show an excess of percolated carbon, as revealed by their electrical conductivity higher than REAC fiber ones [20,60].

It seems evident that hydrogen-poor fibers would highlight high stress exponent favorable for low stress application combined with high $V^*$ constants. These hypothetical and distinct mechanisms would further be evaluated extracting the stress exponent from test performed on dehydrogenated REAC fibers [61,62]. Third generation fibers present such characteristics. Reinforcement with SiC-based fibers of REAC family would better suit shorter usage and high stress or temperature versatility (Fig. 5), due to the lower $n_f$ and $Ea_\tau$ coefficients they display. This being said, given a good woven bundle structure and proper matrix infiltration remain prevailing requirements. It thus become interesting to anticipate, based on above observations, the behavior and potential of alternative (existing or not) SiC-based fibers prior to any time-consuming static fatigue evaluation.

### 4.6 Prediction of static fatigue behaviour

NL101 and AM fiber types were integrated to that end. Filament mechanical properties (Table 2) and bundle structure (Table 4) were above disclosed. NL101 is a high oxygen containing (15.7 at.%) and intermediate hydrogenated (6.3 at.% H) fiber, ancestor of NL200 series with poor mechanical properties. From its composition, free of doping element, it would likely belong to the REAC family. In the other way, AM (13.8 at.% O and 2.7at.% H) has a higher oxygen content than ZMI or Lox-M. Prior to simulation, $n_f$ at 650°C was estimated from figure 7b: 9.9 for NL101 and 12.7 for AM, respectively close to NL207 and Hi-Ni. AM fiber is consequently classified in the STAB group, most likely thanks to the doping element (aluminum) assumed to act similarly to zirconium on chemical stabilization. A $Ea_\tau$ of 180 kJ $mol^{-1}$ is therefore selected for this fiber.

Algorithm results are presented in Table 10 and graphically displayed in Figure 8. NL101 shows a broad scattering ($m_{\tau t}$ of 0.44, similar to Hi-Ni-S, Table 9), associated to its poor mechanical properties and degraded structure. Failure during the initial testing instant would be expected for stresses as low as 300 MPa at 650 °C. Its bundle stress exponent, likewise filament one, would be close to NL207: $n_t$ = 7.2. As far as AM is concerned, virtual tow lifetime distribution is identical to Hi-Ni ($m_{\tau t}$ = 0.75whereas $n_t$ value is similar to ZMI one: $n_t$ = 9.2. With respective $n_f - n_t$ of 2.7 and 3.5, NL101 is similar to NL207 and AM is below the Hi-Ni value. Based on these results the NL101 would be expected to show a poor resistance to SCG and would not be promoted in front of other first generation fibers. AM type is similar to ZMI (Fig 4d) and thus shows a great potential, never explored up to now (*see supplementary document S.5*). This would argue a testing campaign on AM type. Further improvement could be achieved ameliorating the bundle structure. It is worthwhile remaining these SCG coefficient were estimated based on the oxygen and hydrogen content only.

| | NL101 | AM |
|---|---|---|
| $K_{IC}$ (MPa $m^{1/2}$) | 1.2 | 1.2 |
| H (at.%) | 6.3 | 2.7 |
| $n_f$ | 9.9 | 12.7 |
| $\alpha_t$ (%) | 17.0 | 13.7 |
| $A_{1.f}$ 650°C ($m^{1-n/2}$ $MPa^{-n}$ $s^{-1}$) | $2.1 \times 10^{-9}$ | $5.2 \times 10^{-9}$ |
| | Simulation output | |
| $n_t$ | 7.2 | 9.2 |
| $A_{1.t}$ *650°C* ($m^{1-n/2}$ $MPa^{-n}$ $s^{-1}$) | $2.6 \times 10^{-9}$ | $1.5 \times 10^{-9}$ |
| $Ea_\tau$ *(KJ* $mol^{-1}$*)* | 130 | 180 |
| $A_{10.t}$ ($m^{1-n/2}$ $MPa^{-n}$ $s^{-1}$) | $6.82 \times 10^{-2}$ | 79.9 |
| $m_{\tau t}$ | 0.44 | 0.76 |

**Table 10**: SCG parameters for NL101 and AM types, estimated from their chemical composition for 650 °C.

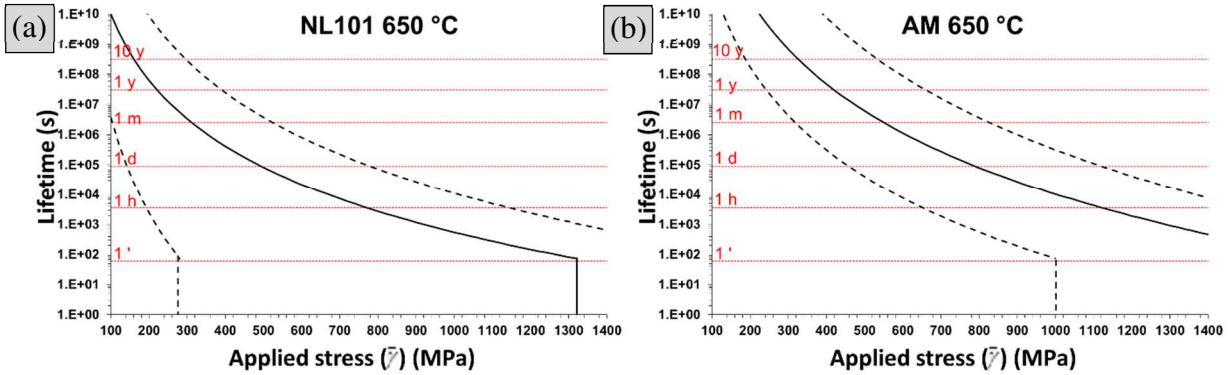


**Fig. 8**: Computed endurance diagram for (a). NL101 and (b). AM tow estimated from the relationship between $n_f$ and the hydrogen content and between $A_{1.f}$ an $n_f$, combined to measured filament strength distribution and tow structure in the algorithm.

A final remark: it is believed $A_{1.f}$ is more accurately related to oxidation resistance. This latter parameter has been the object of a tremendous number of studies in the past decades, covering a broad range of environmental conditions (temperature, environment). However, some discrepancies in testing or measurements make comparative studies questionable [63] and thus such correlation has not been undertaken. It is hence deemed necessary to reinforce the knowledge on SiC fiber oxidation sensitivity (including all fiber types in a true comparative study) in the static fatigue conditions, *i.e.* under ambient air (partial $H_2O$ pressure) at

intermediate temperatures. Effect stress could play on such oxidation kinetic should carefully be reviewed [59]. This will be the object of future investigations.

# 5. Conclusion

Prediction parameters for the delayed failure of 6 different SiC-based tow types, of great relevance for ceramic matrix composite engineering, were assessed by static fatigue under ambient air at intermediate temperature. These coefficients are however known to be pertinent to the tested scale, here multifilament tow scale of limited relevance for fundamental understanding of substrate characteristics. To circumvent this major drawback, an algorithm integrating the filament stress and strength uncertainties to depict the bundle lifetime was reverse operated. Statistical parameters describing filament strength an bundle structure were therefore assessed from a large testing campaign. Stress exponents for single fibers were estimated to range from 7.4 on Lox-M to 13.8 on Hi-Nicalon Type S, systematically subjected to a scale effect ($n_t$<$n_f$) of different extend and structure-related. Lifetime ranking of fiber types is unchanged for filaments and tows, highlighting the superior resistance for intermediate temperature (<1000 °C) of Hi-Nicalon Type S and Tyranno ZMI, over Hi-Nicalon and the other first generation fibers. Any hierarchical approach would however focus on weak tows rather than median values. SPT diagrams were consequently built and show an alternative ranking for weak tows (1% failure probability), in favor of ZMI fiber and discarding the Hi-Nicalon type S. This demonstrates how important it becomes to integrate the lifetime variability and its extend.

SCG parameters for filaments support the existence of two families:

(i). $n_f \geq 12$ gathering Hi-Ni, Hi-Ni-S, ZMI which are chemically stable fibers (low oxygen and hydrogen contents or SiCO phase stabilized by zirconium) and

(ii). $n_f \leq 10$ including NL207, TS, Lox-M which display a weaker stability (high oxygen and hydrogen content, non-stabilized SiCO phase).

Families may involve distinct slow crack growth mechanisms, respectively carbon free oxidation and stress corrosion of SiCO amorphous phase. Relationship to substrate chemistry were proposed and used to give an estimate of NL101 and Tyranno AM static fatigue behavior. These estimates show a great potential with AM fiber type, never evaluated so far. This work marks a step forward in the understanding and simulation of SiC-based bundle behavior under static fatigue conditions, toward the design on purpose of CMC. Perspectives in simulating ceramic matrix composite evolution among time in usage conditions to suit specific application and their versatility (low, medium or heavy duty) are opened. The same methodology would apply to other long fiber types (glass, alumina…) subjected to such delayed failure under subcritical stresses.

## Acknowledgments

The authors acknowledge the financial support of the Snecma Propulsion Solide (now Safran Ceramics) for this work.

## Competing financial interests

The authors declare that they have no competing financial interests.

## References

[1] M. Grenet, Recherches sur la résistance mécanique des verres, Société de l'Encouragement pour l'Industrie nationale 4 (1899) 838−848.

[2] R.J. Charles, Static fatigue of glass II, J. App. Phys. 29(11) (1958) 1554−1560. doi: 10.1063/1.1722992

[3] R.E. Mould, R.D. Southwick, Strength and static fatigue of abraded glass under controlled ambient conditions: I, general concepts and apparatus, J. Am. Ceram. Soc. 42 (1959) 542–547. doi: 10.1111/j.1151-2916.1959.tb13571.x

[4] R.J. Charles, W.B. Hillig, The kinetics of glass failure by stress corrosion, Symposium on Mechanical of Glass and Ways of Improving it, Union Scientifique du Verre, Charleroi, (1962) 511−527.

[5] A.G. Evans, A method for evaluating the time-dependent failure characteristics of brittle materials — and its application to polycrystalline alumina, J. Mater. Sci. 7(10) (1972) 1137−1146. doi: 10.1007/BF00550196

[6] A.G. Evans, S. M. Wiederhorn, Proof testing of ceramic materials—an analytical basis for failure prediction, Int. J. Fract. 10 (1974) 379−392. doi: 10.1007/BF00035499

[7] S.M. Wiederhorn, Moisture assisted crack growth in ceramics, Int. J. Fract. Mech. 4(2) (1968) 171−177.
doi: 10.1007/BF00188945

[8] S.M. Wiederhorn, Subcritical crack growth in ceramics, Bradt R.C., Hasselman D.P.H., Lange F.F. (eds) Fracture Mechanics of Ceramics. Springer, Boston, MA (1974).
doi: 10.1007/978-1-4615-7014-1_12

[9] A.G. Evans, L.R. Russell, D.W. Richerson, Slow crack growth in ceramic materials at elevated temperatures, Metal. Trans. 6A (1975) 707−715.
doi: 10.1007/BF02672290

[10] K.D. McHenry, R.E. Tressler, Subcritical crack growth in silicon carbide, J. Mater. Sci. 12 (1977) 1272−1278.
doi: 10.1007/BF00553618

[11] M.J. Matthewson, C.R. Kurkjian, Environmental effects on the static fatigue of silica optical fiber, J. Amer. Ceram. Soc. 71(3) (1988) 177−183.
doi: 10.1111/j.1151-2916.1988.tb05025.x

[12] F.R. Jones, N.T. Huff, Structure and properties of glass fibres, Handbook of Textile Fibre Structure Natural, Regenerated, Inorganic and Specialist Fibres, 2 (2009) 307−352.
doi: 10.1533/9781845697310.3.307

[13] T. Lube, R.A.G. Baierl, Sub-critical crack growth in alumina – a comparison of different measurement and evaluation methods, BHM 156(11) (2011) 450–456. doi: 10.1007/s00501-011-0035-y

[14] J. Lamon, A micromechanics-based approach to the mechanical behavior of brittle-matrix composites, Comp. Sci. Tech. 61 (2001) 2259–2272. doi: 10.1016/S0266-3538(01)00120-8

[15] W. Gauthier, J. Lamon, Delayed Failure of Hi-Nicalon and Hi-Nicalon S multifilament tows and single filaments at intermediate temperatures (500°-800°C), J. Am. Ceram. Soc. 92(3) (2009) 702–709. doi: 10.1111/j.1551-2916.2009.02924.x

[16] J. Lamon, S. Mazerat, M. R'Mili, Reinforcement of ceramic matrix composites: properties of SiC-based filaments and tows, in P. Narottam, N.P. Bansal, J. Lamon (Eds), Ceramic Matrix Composites: Materials Modelling, and Technology, John Wiley & Sons: Hoboken, NJ, (2015), pp. 3–26. doi: 10.1002/9781118832998.ch1

[17] S.J. Robertson, M.B. RugglesWrenn, R.S. Hay, T. Shilling, R. Mitchell, B. Kroeger, L. Gumucio, Static fatigue of Hi-NicalonTM-S fiber at elevated temperature in air, steam, and sillicic acid-saturated steam, J. Am. Ceram. Soc. 103(2) (2020) 1358–1371 doi: 10.1111/jace.16799

[18] P.L. Swanson, Subcritical crack growth and other time and environment dependent behavior in crustal rocks, J. Geo. Res. 89(B6) (1984) 4137–4152.
doi: 10.1029/JB089iB06p04137

[19] G.J. Qiao, W. Hongjie, J. Zhihao, Comparison between fatigue behavior of some ceramics: a newconcept of intrinsic stress-corrosion exponent $n_0$, Int. J. Fatigue 24 (2002) 499–508.
doi: 10.1016/S0142-1123(01)00175-X

[20] G. Chollon, R. Pailler, R. Canet, P. Delhaes, Correlation between microstructure and electrical properties of SiC-based fibres derived from organosilicon precursors, J. Eur. Ceram. Soc. 18 (1998) 725–33.
doi: 10.1016/S0955-2219(97)00177-5

[21] N. Al Nasiri, N. Ni, E. Saiz, J. Chevalier, F. Giuliani, L.J. Vandeperre, Effect of microstructure and grain boundary chemistry on slow crack growth in silicon carbide at ambient conditions, J. Eur. Ceram. Soc. 35 (2015) 2253–2260.
doi: 10.1016/j.jeurceramsoc.2015.02.020

[22] J. Lamon, M. R'Mili, Resistance to fatigue at intermediate temperature in air for SiC Hi-Nicalon Fibers: statistical distributions of lifetimes and strength degradation, J. Am. Ceram. Soc. 95(11) (2012) 3613–3621.
doi: 10.1111/j.1551-2916.2012.05414.x

[23] A. Laforet, Rupture différée en fatigue statique aux très hautes températures (800°C-1300°C) des fils Hi-Nicalon, des composites Hi-Nicalon/type PyC/SiC et des composites Hi-Nicalon/type PyC/$B_4C$, PhD Thesis, University of Bordeaux, France (2009).

[24] O. Loseille, J. Lamon, Prediction of lifetime in static fatigue at high temperatures for ceramic matrix composites, J. Adv. Mater. Res. 112 (2010) 129−140. doi: 10.4028/www.scientific.net/AMR.112.129

[25] S. Mazerat, R. Pailler, Effect of microstructure and chemical composition on subcritical crack growth in SiC-based fiber tows, Ceram. Int. 47(2) (2021) 2888−2891. doi: 10.1016/j.ceramint.2020.09.052

[26] S. Mazerat, R. Pailler, Delayed failure under static fatigue of Hi-Nicalon bundles: the role of stress dispersion on scale effect, Mater. Let. 294 (2021) 129806 doi: 10.1016/j.matlet.2021.129806

[27] R. Chudoba, M. Vorechovsky, M. Konrad, Stochastic modeling of multi-filament yarns. I. Random properties within the cross-section and size effect, Int. J. Solids Struct. 43 (2006) 413–434. doi: 10.1016/j.ijsolstr.2005.06.063

[28] C. Cluzel, E. Baranger, P. Ladevèze, A.Mouret, Mechanical behaviour and lifetime modelling of self-healing ceramic-matrix composites subjected to

thermomechanical loading in air, Comp A: App. Sci. Manuf. 40(8) (2009) 976–984.
doi: 10.1016/j.compositesa.2008.10.020

[29] C. Laffon, A.M. Flank, P. Lagarde, M. Laridjani, R. Hagege, P. Orly, J. Cotteret, J. Dixier, J.L. Miquel, H. Hommel, A.P. Legrand, Study of Nicalon-based ceramic fibres and powders by EXAFS spectrometry, X-ray diffractometry and some additional methods, J. Mater. Sci. 24 (1989) 1503–1512.
doi: 10.1007/BF02397093

[30] M. Takeda, A. Urano, J.I. Sakamoto, Y. Imai, Microstructure and oxidative degradation behavior of silicon carbide fiber Hi-Nicalon type S, J. Nuclear Mater. 258–263 (1998) 1594–1599.
doi: 10.1016/S0022-3115(98)00223-2

[31] F. Teyssandier, G. Puyoo, S. Mazerat, G. Chollon, R. Pailler, F. Babonneau, Contribution to the understanding of the microstructure of first generation Si-C-O fibers, in: M. Halbig, S. Mathur, T. Ohji, M. Singh (Eds.), Advanced Processing and Manufacturing Technologies for Structural and Multifunctional Materials VI, 33 (2012) Ceram. Eng. Sci. Proc. Wiley, New York pp. 1–11.
doi: 10.1002/9781118217528.ch1

[32] N. Lissart, J. Lamon, Statistical analysis of failure of SiC fibres in the presence of bimodal flaw populations, J. Mater. Sci. 32 (1997) 6107–6117.
doi: 10.1023/A:1018600119250

[33] ISO 19630, Fine ceramics (advanced ceramics, advanced technical ceramics) -- Methods of test for reinforcements -- Determination of tensile properties of filaments at ambient temperature 2021.

[34] S. Mazerat, R. Pailler, Static fatigue of SiC-based multifilament tows at intermediate temperature: the time to failure variability, Int. J. Fatigue (2020) 106072.
doi: 10.1016/j.ijfatigue.2020.106072

[35] S. Mazerat, R. Pailler, Simulating the variability and scale effect for slow crack growth in Hi-Nicalon SiC-based tows: a parametric study, J. Eur. Ceram. Soc. (2021).
doi: 10.1016/j.jeurceramsoc.2021.07.032

[36] European Standard, determination of distribution of tensile strength and of tensile strain to failure of filaments within a multifilament tow at ambient temperature, CEN TC 184, ENV 1007-5 (1998).

[37] P. Forio, F. Lavaire, J. Lamon, Delayed failure at intermediate temperature (600 °-700 °C) in air in silicon carbide multifilament tows, J. Am. Ceram. Soc. 87 (2004) 888–893.
doi: 10.1111/j.1551-2916.2004.00888.x

[38] S. Mazerat, A. Delehouze, R. Pailler, Delayed failure prediction of SiC-based bundles: the impact of sampling size, Int. J. Fatigue 138 (2020) 105694. doi: 10.1016/j.ijfatigue.2020.105694

[39] J.D. Sullivan, P.H. Lauzon, Experimental probability estimators for Weibull plots, J. Mater. Sci. Letters 5 (1986) 1245−1247. doi: 10.1007/BF01729379

[40] B. Bergman, On the estimation of the Weibull modulus, J. Mater. Sci. Let. 3 (1984) 689−692. doi: 10.1007/BF00719924

[41] I. J. Davies, Confidence limits for Weibull parameters estimated using linear least squares analysis, J. Eur. Ceram. Soc. 37(15) (2017) 5057−5064. doi:10.1016/j.jeurceramsoc.2017.05.051

[42] V. Calard, J. Lamon, Failure of fiber bundles, Comp. Sci. Tech. 64 (2004) 701−710. doi: 10.1016/j.compscitech.2003.07.003

[43RMi96] M. R'Mili, T. Bouchaour, P. Merele, Estimation of Weibull parameters from loose-bundle tests, Comp. Sci. Technol. 56 (1996) 831−834. doi: 10.1016/0266-3538(96)00028-0

[44] J. Lamon, M. R'Mili, Damage and failure of SiC fiber tows during environment activated slow crack growth: residual behavior and strength-probability-time diagrams, Acta Mater. 131 (2017) 197–205.
doi: 10.1016/j.actamat.2017.03.073

[45] H.E. Daniels, The statistical theory of the strength of bundles of threads. I, Proc. Royal Soc. 138 (1945) 405–435.
doi: 10.1098/rspa.1945.0011

[46] B.D. Coleman, On the strength of classical fibers bundle, J. Mech. Phys. Solids 7 (1958) 60–70.
doi: 10.1016/0022-5096(58)90039-5

[47] A. Hansen, P.C. Hemmer, S. Pradhan, The Fiber Bundle Model: Modeling Failure in Materials, Weinheim, Germany: Wiley-VCH, (2015).
doi:10.1002/9783527671960

[48] S. Mazerat, R. Pailler, Statistical data for the tensile properties and static fatigue of SiC-based bundles, Data Brief 32 (2020) 106166.
doi: 10.1016/j.dib.2020.106166

[49] S. Mazerat, G. Puyoo, G. Chollon, F. Teyssandier, R. Pailler, S. Loison, E. Philippe, Composition and reactivity of various silicon carbide fibers, HTCMC8 Ceram. Trans. 248 (2014) 113–123.
doi: 10.1002/9781118932995.ch13

[50] S. Mazerat, R. Pailler Dataset on fractographic analysis of various SiC-based fibers, Data Biref 34 (2021) 106676.
doi: 10.1016/j.dib.2020.106676

[51] R. Danzer, T. Lube, P. Supancic, R. Damani, Fracture of ceramics, Adv. Eng. Mater. 10(4) (2008) 275−298.
doi: 10.1002/adem.200700347

[52] S. Mazerat, A. Delcamp, R. Pailler, J. Lamon, H. Plaisantin, Improvement of silicon carbide fibers mechanical properties by $Cl_2$ etching, J. Eur. Ceram. Soc. 38(16) (2018) 5301−5310.
doi: 10.1016/j.jeurceramsoc.2018.06.026

[53] R.W. Davidge, J.R. McLaren, G. Tappin, Strength-probability-time (SPT) relationships in ceramics, J. Mat. Sci. 8(12) (1973) 1699−1705.
doi: 10.1007/BF00552179

[54] W. Gauthier, Rupture différée en fatigue statique, aux températures intermédiaires (<800 °C), de fils et de fibres à base de carbure de siliciuum, PhD thesis University of Bordeaux, France (2006)

[55] A.R. Bunsell, M.-H. Berger, Fine diameter ceramic Fbres, J. Eur. Ceram. Soc. 20 (2000) 2249−2260.
doi: 10.1016/S0955-2219(00)00090-X

[56] K. Igashira, Decomposition and Oxidation Resistance of Si-M(Ti, Zr)-C-O Fibers at Elevated Temperature, 27th Annu. Cocoa Beach Conf. Adv. Ceram. Compos. B Ceram. Eng. Sci. Proc. (2003) 255–260.
doi: 10.1002/9780470294826.ch37

[57] S.M. Wiederhorn, L.H. Boltz, Stress corrosion and static fatigue of glass, J. Am. Ceram. Soc. 53(10) (1970) 543–548.
doi: 10.1111/j.1151-2916.1970.tb15962.x

[58] I.W. Smith, The intrinsic reactivity of carbons to oxygen, Fuel 57 (1978) 409–414.
doi: 10.1016/0016-2361(78)90055-8

[59] W. Gauthier, F. Pailler, J. Lamon, R. Pailler, Oxidation of silicon carbide fibers during static fatigue in air at intermediate temperatures, J. Am. Ceram. Soc. 92(9) (2009) 2067–2073.
doi: 10.1111/j.1551-2916.2009.03180.x

[60] S. Mazerat, J. Lacroix, B. Rufino R. Pailler, Carbon derived from silicon carbide fibers, a comparative study, Mater. Today Com. 19 (2019) 177–185.
doi: 10.1016/j.mtcomm.2019.01.013

[61] O. Greck, J.P. Viricelle, D. Bahloul-Hourlier, P. Goursat, M. Dalbin, S. Thomin, A.M. Flank, SiC-based ceramic fibres: thermal stability and oxidation behaviour, Key Eng. Mater. 132–136 (1997) 1950–1953.

doi: 10.4028/www.scientific.net/KEM.132-136.1950

[62] J.P. Viricelle, D. Bahloul-Hourlier, P. Goursat, Oxidation behaviour of SiC based fiber, Key Eng. Mater. 127–131 (1997) 203–210.
doi: 10.4028/www.scientific.net/KEM.127-131.203

[63] M. Wilson, E.J. Opila, A review of SiC fiber oxidation with a new study of Hi-Nicalon SiC fiber oxidation: Advanced Engineering Materials. 18 (10) (2016) 1698–1709.
doi: 10.1002/adem.201600166.